REMOTE SENSING FOR DETECTION OF RHIZOCTONIA CROWN AND ROOT ROT OF SUGARBEET

Ashok K. Chanda[1], Ian V. MacRae[2], Tim Baker[3], Jason R. Brantner[3], Nicole Dudycha[3]

[1]Dept. of Plant Pathology, University of Minnesota, [2] Dept. of Entomology, University of Minnesota [3]University of Minnesota, Northwest Research and Outreach Center

Rhizoctonia crown and root rot (RCRR), caused by *Rhizoctonia solani* AG 2-2, is becoming more frequent and widespread in the sugarbeet-growing regions of Minnesota and North Dakota. In this region, symptoms of RCRR typically begin at about 8 weeks after planting and continue to develop until harvest. Infected plants occur sporadically or in large portions of the field. Advances in remote sensors and vehicle platforms have regenerated interest in within-season aerial mapping/detection of RCRR.

Remotely assessing plant health by measuring the reflectance of incident electromagnetic radiation is well established (Nilsson, 1995). Evaluating the relative canopy reflectance of specific wavelengths can provide insight into the impacts of insects (e.g. Alves et al. 2015), nutrient state (e.g. Felderhof & Gillieson 2012) and disease (well-reviewed in Oerke et al. 2014). Specifically, spectral reflectance has been demonstrated to show the presence of *Rhizoctonia solani* AG 2-2 prior to the development of visible symptoms (Reynolds et al. 2009 and 2012).

Detection of plant diseases is based on pathogen-induced degradation of chlorophyll and subsequent deterioration of palisade parenchyma cells in the leaf (Inoue, 2003). Chlorophyll absorbs red wavelengths of energy, so its degradation results in increased reflectance in the Red wavelengths (~620nm-680nm). Parenchyma cells reflect Near-Infrared (NIR) energy (~700nm-1100nm) and their deterioration results in lowered reflectance of NIR. The comparative ratio of these wavelengths can, therefore, provide insight into the level of stress being endured by a plant. Remotely sensed plant reflectance has been used for detecting sugarbeet diseases including Rhizomania (Steddom et al., 2005), Cercospora leaf spot (Steddom et al., 2005), sugarbeet cyst nematode (Schmitz et al., 2003), and RCRR (Laudien et al., 2003, 2004, 2006, Reynolds et al. 2009 and 2012). Most early research detected RCRR at the end of the growing season but did not address earlier-season detection of the disease or the relationship of reflectance to severity of root rot symptoms. There have been indications, however, that earlier identification of infection may be possible. Reynolds et al. (2009 and 2012) found that specific wavelengths and vegetative indices were more closely associated with plants showing lower root ratings of the disease. While several indices were correlated with disease severity, the narrowband *modified Spectral Ratio* (mSR) index, calculated as [(*R*750-*R*445)/(*R*705-*R*445) where *R* is the measure of reflection in that wavelength], appeared to allow for earlier detection of RCRR than did wideband indices such as *Normalized Difference Vegetative Index* (NDVI) or *Optimized Soil Adjusted Vegetative Index* (OSAVI) that were correlated with RCRR infection severity (Reynolds 2010). Unfortunately, this research effort was not able to further pursue and refine the further diagnostic capabilities of reflectance measurements.

The objectives of this study were 1) to establish baseline hyperspectral reflectance data associated with disease severity for RCRR of partially resistant and susceptible sugarbeet varieties 2) to identify the most sensitive and strongest diagnostic reflectance data (wavelengths) for detection of disease.

Materials and Methods:

Field experiments and design - In 2016/ and 2017 sugarbeet varieties partially resistant (4.0 rating) and susceptible (4.7 rating) to RRCR were planted in field plots (4 replications) at the University of Minnesota, NWROC. Plots were 35 ft long by 4 rows wide. In inoculated plots, *Rhizoctonia solani* AG 2-2 IIIB infested barley grain (at three different rates; 20 kg/ha, 40 kg/ha, and 60 kg/ha) was broadcast at planting to mimic naturally infested Rhizoctonia fields with low, medium, and high levels. For one treatment, near canopy closure, plants were inoculated (four center rows of six-row plots) with *R. solani* AG 2-2 IIIB infested barley grains by placing two whole kernels about 1-inch below the soil surface and adjacent to the root. One treatment included non-inoculated control. Plots were split into a 22-ft section (4-rows wide) for visual assessment of disease (0-7 scale, 0 = root clean, 7 = root completely rotted), with the remaining 13-ft length (4-rows wide) left for reflectance imagery. At each sample date, twelve plants were randomly

selected and pulled from one end from the 22' section of each plot and their roots visually assessed for disease symptoms. Simultaneously, one of the oldest leaves from that plant was assessed for reflectance using the specroradiometer.

Reflectance data - Hyperspectral reflectance of individual leaves on plants was obtained using an Ocean Optics Flame hyperspectral radiometer. The Ocean Optics Flame is sensitive to the visual and near-infrared wavelengths (VIS/NIR) typically raning from ~350nm to ~1100nm, however due to signal loss at the extreme edges of the sensor, only wavelength responses between 400nm – 950nm were used in data analyses. A self-illuminated, leaf-clip sensor was used with the Ocean Optics radiometer, the illuminator of which provided light over all wavelengths that the senor can read (350nm-1100nm). Consequently, the absolute reflectance, within sensitivity limits, of the plant's leaf surface could be assessed as the percent of light energy being reflected (reflectance). Multispectral imagery was also obtained using multi-sensor arrays which included a standard visual RGB camera and 3 cameras sensitive to specified wavelengths in the Near-InfraRed (NIR) (Sentera, Minneapolis MN). These sensors were mounted on small Unmanned Aerial Systems (i.e. drones). Measurements were obtained weekly starting at 8 weeks after planting and 2 weeks after whole barley inoculation (~11 am to 2 pm).

Disease data - Disease ratings were taken from sampled plants at the same time as reflectance data was measured. Tap roots were visually assessed for RCRR using a 0-to-7 scale (Ruppel et al. 1979), where 0 = no visible lesions; 1 = superficial, scattered inactive lesions; 2 = shallow, dry rot cankers or active lesions on ≤5% of root surface; 3 = deep dry-rot cankers at crown or extensive lateral lesions affecting 6 to 25% of the root; 4 = rot affecting 26 to 50% of tap root, with cracks and cankers up to 5 mm deep; 5 = 51 to 75% of tap root blackened, with rot extending into interior and roots usually misshapen with cracks and rifts; 6 = entire root blackened except extreme tip; and 7 = root 100% rotted and foliage dead.

Data analyses – Disease ratings were assigned the percentage of root covered with necrosis associated with that rating (i.e. rating of: 0=0%, 1=2.5%, 2=5%, 3=25%, 4= 50%, 5=75%, 6=95%, 7=100% root covered). The percent of root covered by necrosis values (% necrosis) were then transformed using ArcSine of the square root to normalize the data. To assess the wavelengths of reflected light most influenced by RCRR infection, individual wavelengths (from 400nm to 950nm) were correlated with %necrosis for all individual plants at all dates. The respective correlation coefficients from wavelengths and disease rating were used to calculate the Akaike Information Criteria (AIC) values which were used to rank each wavelength for its ability to predict RCRR disease rating (Akaike 1974). The AIC is a metric used to evaluate best fit, in this case, which wavelengths are most closely associated with RCRR disease rating. Lower AIC ratings indicate better fit (Burnham and Anderson, 2003). The AIC values were then compared using a Relative Likelyhood calculation (RL_i = exp((lowest AIC - AIC_i)/2), where RL_i is the Relative Likelyhood at a specific wavelength (i) of it being best fit of all AICs (i.e. most closely associated with RCRR infection).

Results and Discussion:

Plots were sampled 7/10, 7/13, 7/14, 7/18, 7/20, 7/26, 8/02, 8/08, and 8/15. Unfortunately, due to equipment failure, data from 7/26 had to be discarded from the analyses. All other dates had expressed symptoms in inoculated plots (for both resistant and susceptible varieties), resulting a gradient of infection throughout the season.

The leaf clip readings from the Ocean Optics Flame Spectroradiometer returned the percent reflectance of light in wavelengths from 350nm to 1100nm (fig 1). Unfortunately, the design of CCD-based sensors, such as those used in most VIS/NIR spectroradiometers, results limitations at the extreme edges of the sensor's range, resulting in increased 'noise' and loss of signal integrity. As can be seen in Fig 1, the signal to noise ratio of data below 450nm and above 950 nm deteriorates rapidly. Consequently, we decided to use reflection responses at wavelengths from 450nm-950nm only for analyses (fig 2).

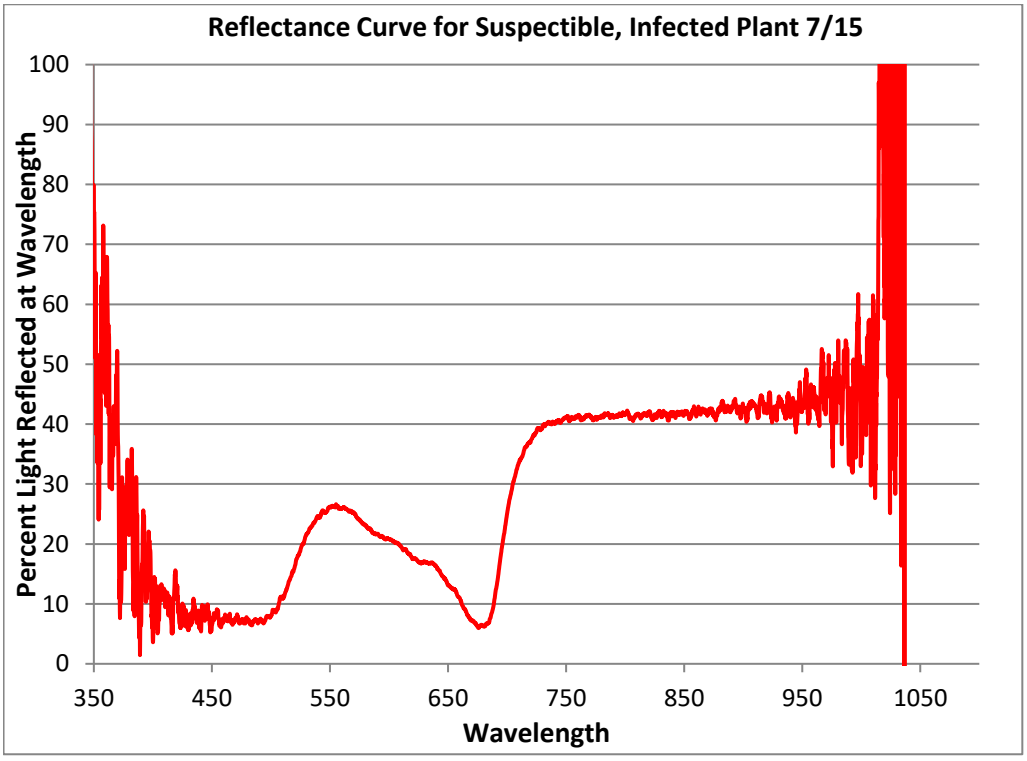

Figure 1. Typical complete reflectance curve as measured by leaf clip sensor attached to Ocean Optics spectroradiometer. Note decreasing signal to noise at extreme edges of sensor's range of sensitivity.

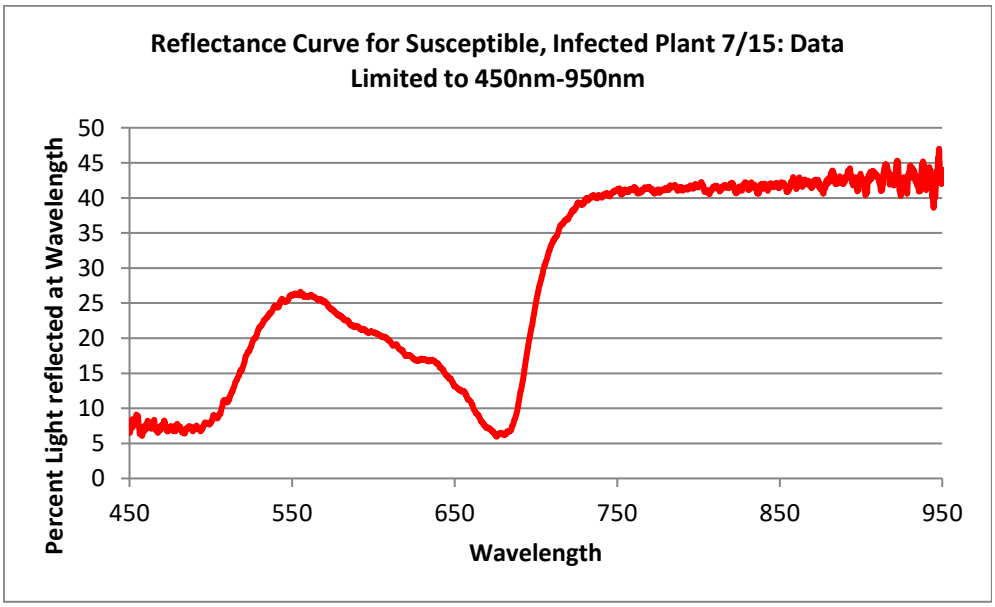

Figure 2. Typical spectral reflectance curve as measured by leaf clip sensor attached to Ocean Optics spectroradiometer, data has been limited to wavelengths between 450nm=-950nm.

A multiple correlation incorporating date and variety was used to assess the disease ratings of 12 plants per plot at each date (40 plots X 12 plants = 480 plants per sample date) with all 500 analyzed wavelengths (450nm-950nm) (a total of 240,000 wavelengths associated with disease ratings were assessed at each sample date). The resulting correlations were assessed for association to RCRR disease rating using AIC, AIC's were plotted against assessed wavelength for all dates (fig 3) (resulting in a total of 1,680,000 wavelengths associated with disease ratings – this multiple regression will stress computing limits!). The lowest AIC value on the AIC vs Wavelengths graph is considered to be the most important (i.e. in our case, the wavelengths most closely associated with RCRR infection).

It is important to note that the AIC is not a statistic and therefore cannot be directly compared, its units depend on the value of the coefficients in the association analysis and on the number of parameters in the model being assessed. To compare AIC values of wavelengths to assess which wavelengths was most closely associated with RCRR infection, a Relative Likelihood analysis was conducted (fig 4).

There is increasing variation in AIC values above 750 nm, this reflects the variation in reflectance values found in that range; there was no clear association of reflection of NIR above 750 and RCRR infection. The lowest AIC values appear just below 700nm (the range between red and NIR wavelengths). The relative Likelihood analysis indicates that, in our data, the wavelengths most closely associated with RCRR infection occur in a narrow band of approximately 20nm, centered around 689nm. The next highest peak occurred at 698 nm (although this may actually be a part of the 689 narrow bandwidth. Most sources consider these values to be technically red wavelengths, although some sources

AIC = -2*LN(ʎ) + (2*P)

Where:

ʎ = metric of association (coefficient) and

P = # parameters in the model

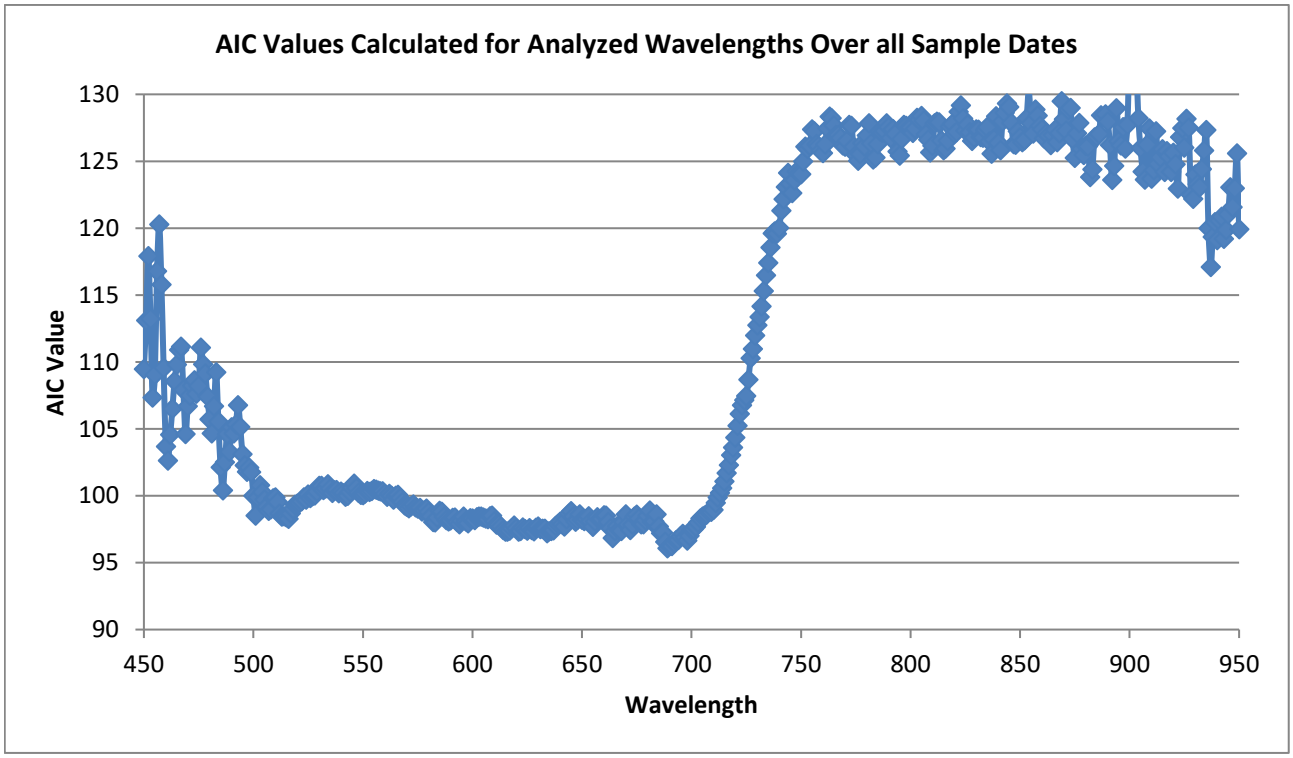

Figure 3. Akaike Information Criteria (AIC) values calculated for analyzed wavelengths over all sample dates. The lowest AIC value is considered the most influential in the relationship (i.e. the wavelengths most closely associated with RCRR infection).

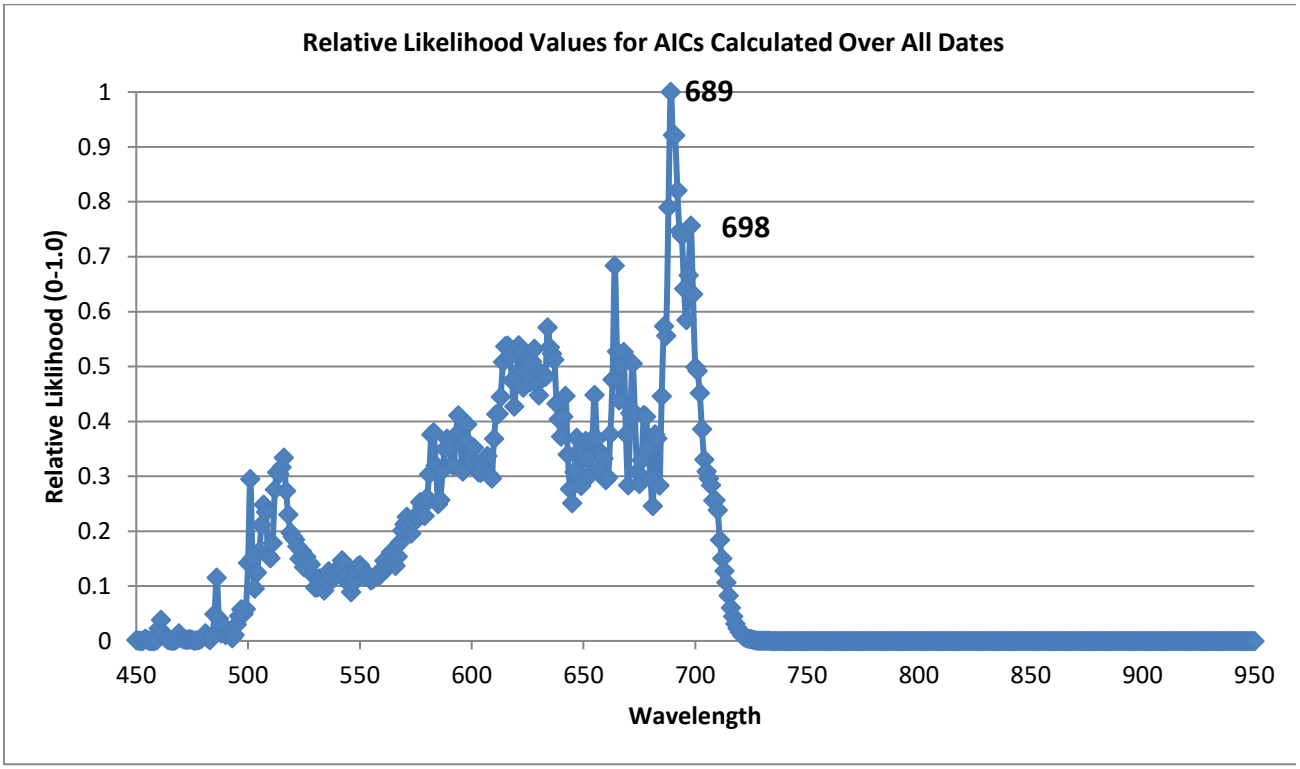

Figure 4. Relative Likelihood results for AICs calculated for all wavelengths and disease ratings over all dates. The wavelengths most closely associated with RCRR infection in our data are 689 (surrounded by a narrow bandwidth or ~20nm) and 698. An additional series of wavelengths well in the red wavelength range also show high relative likelihoods of being associated with RCRR infection.

place them in the low near-infrared. In either case, this range of wavelengths where red and NIR abut, sometimes inaccurately called the 'Red Edge', is an area where stress reactions in plants often affect the leaf's ability to reflect solar energy. So these results are not surprising. In addition to the narrow band around 689, there are several groups of wavelengths in the range of red wavelengths that show high relative likelihood of being associated with RCRR infection (582nm-602nm, 615nm-634nm, and a very narrow band between 663nm-665nm). Results from aerial imagery from VIS/NIR multi-sensor arrays and Forward Looking Infrared (FLIR) thermal cameras (e.g. fig 5) from all dates are still being analyzed. Results from these sensors will be combined with the reflection data to refine the ability to remotely sense Rhizoctonia Crown and Root Rot.

Conclusions:

In 2017, we found that RCRR does significantly affect the reflection characteristics of infected plants. The data in this study indicates that the most effective wavelengths to assess RCRR infection are a 20nm band centered around 689nm with additional narrow bands of wavelengths in other areas of the red wavelengths. These wavelengths may provide the best potential for the development of RCRR sensors, although additional data from aerial VIS/NIR and thermal imagery may provide significant improvement.

Acknowledgements

We thank Jeff Nielsen, Hal Mickelson, Josie Dillon, and student workers Tim Cymbaluk, Brandon Kasprick, and Muira MacRae; the University of Minnesota, Northwest Research and Outreach Center, Crookston for providing land, equipment and other facilities.

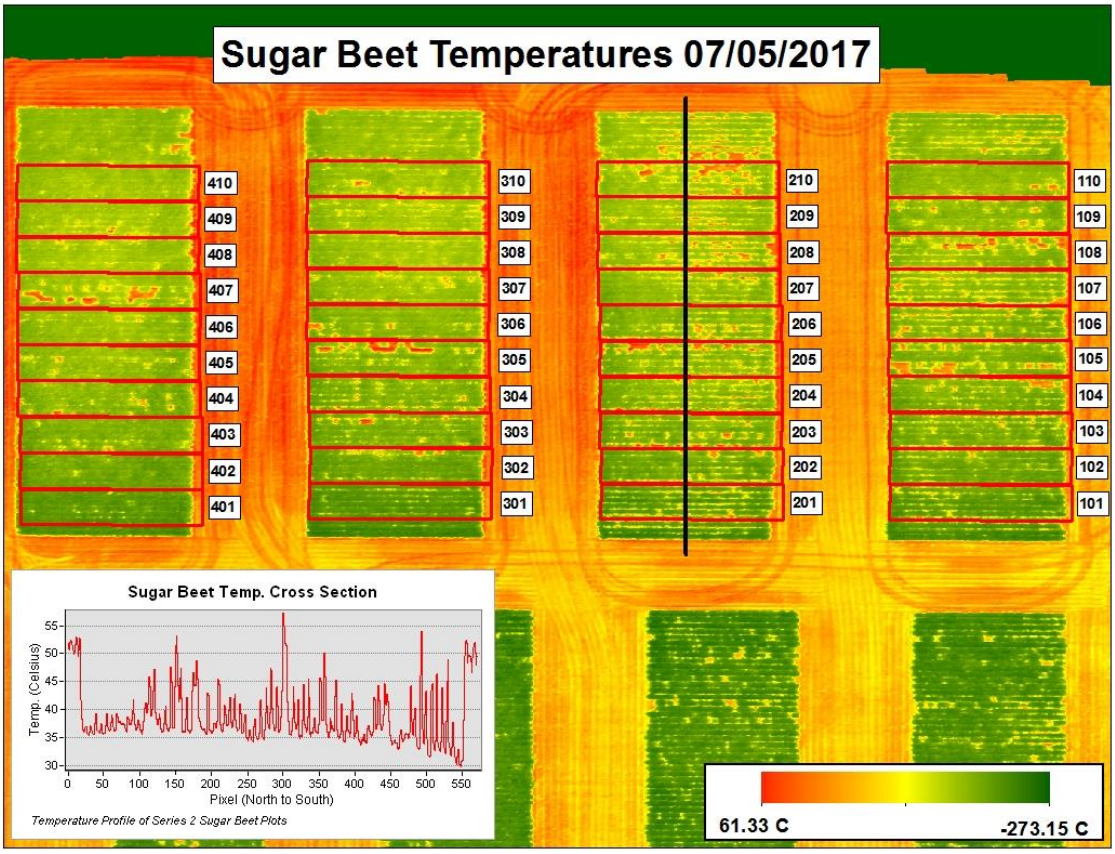

Figure 5. Example of Forward Looking Infrared (FLIR) image or research plots 7/05/2017. Analyses of FLIR imagery is still ongoing; addition of canopy temperatures estimated from these data is anticipated to increase predictive accuracy of identification of RCRR infection.

Literature Cited

Alves, T. M., I. V. MacRae, and R. L. Koch. 2015. Soybean aphid (Hemiptera: Aphididae) affects soybean spectral reflectance. Journal of Economic Entomology, DOI: http://dx.doi.org/10.1093/jee/tov250.

Akaike, H., 1974. A new look at the statistical model identification. IEEE Trans. Automat. Contr. 19, 716–723. doi:10.1109/TAC.1974.1100705

Burnham, K.P. and Anderson, D.R., 2003. *Model selection and multimodel inference: a practical information-theoretic approach*. Springer Science & Business Media.

Felderhof, L. and Gillieson, D. 2012. Near-infrared imagery from unmanned aerial systems and satellites can be used to specify fertilizer application rates in tree crops. Canadian Journal of Remote Sensing, 37(4): 376-386.

Inoue, Y. 2003. Synergy of remote sensing and modeling for estimating ecophysiological processes in plant production. Plant Production Sci. 6:3-5.

Laudien, R. G. Bareth, and R. Doluschitz. 2003. Analysis of hyperspectral field data for detection of sugar beet diseases. Proc. EFITS Conf, 2003.

Laudien, R., G. Bareth, and R. Doluschitz. 2004. Comparison of remote sensing based analysis of crop diseases by using high resolution multispectral and hyperspectral data – case study: *Rhizoctonia solani* in sugar beet. Pages

670-676 *in*: Proc. 12th Int. Conf Geoinformatics-Geospatial Information Research: Bridging the Pacific and Atlantic, Univ. Gavle, Sweden, 7-9 June 2004.

Laudien, R., K. Burcky, R. Doluschitz, and G. Bareth. 2006. Establishment of a web-based spectral database for the analysis of hyperspectral data – case study: *Rhizoctonia solani*-inoculated sugarbeets. Zuckerindustrie 131:164-170.

Nilsson, H.E. 1995. Remote sensing and image analysis in plant pathology. Annu. Rev. Phytopathology 15:489-527.

Oerke, E. C., Mahlein, A. K., & Steiner, U. (2014). Proximal Sensing of Plant Diseases. In *Detection and Diagnostics of Plant Pathogens* (pp. 55-68). Springer Netherlands.

Reynolds, G. J. 2010. Remote sensing for detection of Rhizoctonia crown and root rot in Sugar Beet and the impact of the disease on chlorophyll Content. Dissertation submitted to the University of Minnesota.

Reynolds, G.J., C.E. Windels, I.V. MacRae, and S. Laguette. 2009. Hyperspectral remote sensing for detection of Rhizoctonia crown and root rot in sugar beet. Phytopathology 99(6): s108-s108.

Reynolds, G.J., C.E. Windels, I.V. MacRae, and S. Laguette. 2012. Remote sensing for assessing Rhizoctonia crown and root rot in sugar beet. Phytopathology 96(4): 497-505.

Ruppel, E.G., C.L. Schneider, R.J. Hecker, and G.I Hogaboam. 1979. Creating epiphytotics of Rhizoctonia root rot and evaluating for resistance to Rhizoctonia so/ani in sugarbeet field plots. Plant Dis. 63:518-522.

Schmitz, A., S. Kiewnick, J. Schlang, K. Schmidt, and R.A. Sikora. 2003. Use of remote sensing to identify the spatial distribution of the sugar beet cyst nematode *Heterodera schachttii*. Pages 561-562 In: Program book of the Joint Conference of ECPA-ECPLF, A. Werner and A. Jarfe (Hrsg.)

Steddom, K., M. W. Bredehoeft, M. Khan, and C. M. Rush. 2005. Comparison of visual and multispectral radiometric disease evaluations of Cercospora leaf spot of sugar beet. Plant Disease. 89(2):153-158.

Xu, J., & B. Su. 2017. Significant remote sensing vegetative indices: a review of developments and applications. J. of Sensors 2017. https://doi.org/10.1155/2017/1353691.